

RESEARCH ARTICLE

10.1002/2013JD020919

Key Points:

- Examine the CTHs and cloud top microphysics by CloudSat and CALIPSO
- Clouds where CloudSat-determined CTHs are larger than CALIPSO ones are revealed
- Existence of such clouds implies the cloud tops consist of large particles

Correspondence to:

Hajime Okamoto,
okamoto@riam.kyushu-u.ac.jp

Citation:

Hagihara, Y., H. Okamoto, and Z. J. Luo (2014), Joint analysis of cloud top heights from CloudSat and CALIPSO: New insights into cloud top microphysics, *J. Geophys. Res. Atmos.*, 119, doi:10.1002/2013JD020919.

Received 20 SEP 2013

Accepted 16 DEC 2013

Accepted article online 20 DEC 2013

Joint analysis of cloud top heights from CloudSat and CALIPSO: New insights into cloud top microphysics

Yuichiro Hagihara¹, Hajime Okamoto¹, and Zhengzhao Johnny Luo²

¹Research Institute for Applied Mechanics, Kyushu University, Fukuoka, Japan, ²Department of Earth and Atmospheric Sciences and NOAA CREST Institute, City College of New York, CUNY, New York, New York, USA

Abstract We examined the differences in the cloud top heights (CTHs) detected by the CloudSat radar and Cloud-Aerosol Lidar and Infrared Pathfinder Satellite Observation (CALIPSO) lidar. Theoretical estimates have shown that CloudSat has higher sensitivity than CALIPSO does when large particles exist. In such case it might be possible that CloudSat-determined CTHs are larger than CALIPSO-determined CTHs. We compared the global distribution of CTHs detected by CloudSat and CALIPSO (version 3, V3) using our cloud mask schemes after carefully selecting data during September–November 2006. The global mean fraction of clouds where CloudSat-determined CTHs were larger than CALIPSO-determined CTHs turned out to be unexpectedly large. The fractions were 26% and 39% at low level and midlevel, and the corresponding CTH differences were 0.56 km and 0.86 km, respectively. On the western coasts of continents, these clouds occurred within temperature inversions. Accounting for the differences in sensitivity to particle size between CloudSat and CALIPSO, the existence of such clouds indicates that the cloud tops consist of large particles with small number concentration. The discovery of such clouds was revealed by our joint analysis of CloudSat and CALIPSO. When the standard vertical feature mask (VFM) V3 was used, these clouds were also found but the fractions were less pronounced. The differences were partly attributed to the overestimation of cloud fraction in the VFM V3, although the degree of misidentification in V3 was reduced compared with that of V2.

1. Introduction

Clouds play an important role in Earth's changing climate because they strongly influence the radiative heating and hydrological cycle [e.g., Stephens, 1999]. To adequately evaluate the global energy budget, reliable global observations of the vertical distribution of both macrophysical and microphysical properties of the clouds are crucial. However, passive satellite observations have not been able to resolve cloud vertical structures in the past. They have also suffered uncertainties related to the difficulty in determining cloud top heights (CTHs), especially over polar regions. Recent advances in spaceborne active measurement offer an opportunity to assess these uncertainties [Mahesh *et al.*, 2004; Wylie *et al.*, 2007; Ackerman *et al.*, 2008].

In general, spaceborne lidar is believed to have higher sensitivity to small particles in typical cloud top nucleation zones compared with cloud radar. It is therefore considered more suitable for the determination of CTHs than radar. Spaceborne lidar has been used to validate the passive sensor-based retrievals of CTHs [e.g., Holz *et al.*, 2008]. On the other hand, theoretical estimates have shown that cloud radar might have higher sensitivity to relatively large particles present near the cloud tops than does lidar [Okamoto *et al.*, 2010]. Thus, it is possible that radar-determined CTHs are greater than lidar-determined CTHs. However, this scenario has never been explored before, at least not from space, so its global distribution is unknown.

The CloudSat satellite carries a Cloud Profiling Radar (CPR) [Stephens *et al.*, 2008], and the Cloud-Aerosol Lidar and Infrared Pathfinder Satellite Observation (CALIPSO) platform carries the Cloud-Aerosol Lidar with Orthogonal Polarization, a two-wavelength polarization lidar [Winker *et al.*, 2009]. These satellites are also components of the A-train satellite constellation [Stephens *et al.*, 2002]. They provide a unique opportunity to compare two independently derived CTH data sets. Several CTH intercomparison studies using CloudSat and CALIPSO measurements had been performed previously [Weisz *et al.*, 2007; Mace *et al.*, 2009; Wu *et al.*, 2009]. These studies relied on a "vertical feature mask" (VFM) product (version 2, V2) as a cloud mask for CALIPSO [Vaughan *et al.*, 2009; Liu *et al.*, 2009]. This product occasionally labels remaining noise after onboard subtraction of the background signal or dense aerosols as cloud [Hagihara *et al.*, 2010]. The VFM is also known to overestimate

the cloud regions detected by CALIPSO [e.g., *Marchand et al.*, 2008; *Holz et al.*, 2008]. Therefore, the CALIPSO team released a reprocessed product version 3 (V3) that corrected these issues. However, whether the issues in V2 were corrected in V3 have not yet been investigated.

Here we carefully analyzed CloudSat and CALIPSO data to find out whether there are cases where CTHs are greater in CloudSat than in CALIPSO. We first compared our cloud mask scheme, developed by *Hagihara et al.* [2010], with both the previous release (V2) and the current release (V3) of the VFM. Next, we compared the CTHs derived by CloudSat and CALIPSO using our cloud mask during September–November 2006. Global statistics were examined using the mask scheme and the VFM V3 results. We also inferred the differences in the microphysics of cloud top regions between CTHs detected by sensors from CloudSat and CALIPSO.

Section 2 describes the CloudSat and CALIPSO data, the cloud mask schemes used to determine CTHs, and the comparisons of our cloud mask results with the VFM, followed by a definition of cloud types in light of the CTH differences. Section 3 gives the results of the CloudSat and CALIPSO CTH comparison in detail, including examples where the CloudSat CTHs are higher than the corresponding CALIPSO CTHs. The global distributions of the fraction, mean CTH differences, mean cloud top temperature (CTT) differences, and global statistics of each cloud type are summarized in section 4. Section 5 compares the radar reflectivity factor (Z_e) and the backscattering coefficient (β) at 532 nm in cloud top regions for each type to infer the difference in the cloud microphysics. Finally, in section 6, we summarize the results.

2. Data and Definitions of Cloud Types

We used the CloudSat Z_e (the standard geometrical profile of cloud product, 2B-GEOPROF, release R04) and CALIPSO lidar β at 532 nm (Lidar Level 1B, V3) data with atmospheric profile data from European Centre for Medium-Range Weather Forecasts (ECMWF) analyses.

The CTHs were determined by the cloud mask scheme for CloudSat (hereafter referred to as the C1 mask) and CALIPSO (hereafter referred to as the C2 mask). These schemes were originally developed and tested for shipborne cloud radar and lidar observations by *Okamoto et al.* [2007] in midlatitudes and by *Okamoto et al.* [2008] in the tropics. They were modified for application to CloudSat and CALIPSO data [*Hagihara et al.*, 2010]. The C1 mask uses the CPR Level 2B-GEOPROF cloud mask [*Marchand et al.*, 2008]. We recognize bins with cloud mask level ≥ 20 as cloud bins. These are estimated to have a false-positive probability of 5%. The C2 mask was different from the official CALIPSO cloud mask, i.e., the CALIPSO Lidar Level 2 VFM [*Vaughan et al.*, 2009; *Liu et al.*, 2009]. We first applied a threshold of the total backscattering coefficient at 532 nm to the original resolution of the CALIPSO level 1B data (30 m vertical and 333 m horizontal at altitudes < 8.2 km, and 60 m vertical and 1 km horizontal at altitudes > 8.2 km). The threshold depends on the altitude, the molecular signal derived from ECMWF data, and the remaining noise signal estimated from signals at an altitude of 19–20 km. Next, the spatial continuity test was conducted using the surrounding 5×5 bins at altitudes < 5 km and 9×9 bins at altitudes > 5 km. The cloud mask results for the original resolution were then averaged vertically over 240 m and horizontally over 1.1 km to give each profile the same resolution as CloudSat. In this procedure, we exclude data for which the along-track and cross-track distance between the footprints of CloudSat and CALIPSO exceeds 0.55 and 0.7 km, respectively, to avoid spatial mismatches. The minimum and maximum heights above mean sea level were 0 and 20 km, respectively. As a result, the averaged cloud mask results (i.e., the C1 and C2 results) for the CloudSat grid could take values between 0 and 1. To avoid spurious signals caused by noise, we applied another threshold: If the C1 and C2 mask values exceeded 0.5, we considered the pixel to be cloud. Although CloudSat CPR is highly sensitive to the presence of precipitation and drizzle [*Haynes et al.*, 2009], a threshold is utilized to identify them in general [e.g., *Sassen and Wang*, 2008]. However, precipitation or drizzle is not observed above clouds. Therefore, it does not play a role in the detection since we examine cloud top regions.

As noted above, the VFM V2 [*Vaughan et al.*, 2009; *Liu et al.*, 2009] sometimes made a false detection through the scheme's horizontal averaging procedure and also misclassified noise or aerosols as cloud (and vice versa). *Hagihara et al.* [2010] showed that our cloud mask results had less contamination by remaining noise or aerosol signals compared with those of the VFM. We also compared the zonal-mean cloud coverage for the topmost layer detected by our C2-mask scheme, the VFM, our combined C1/C2 scheme, and collocated Aqua Moderate Resolution Imaging Spectroradiometer (MODIS) results [*Menzel et al.*, 2008]. The C2, C1/C2, and MODIS results were similar for total cloud coverage, but the VFM result was different: Because of possible

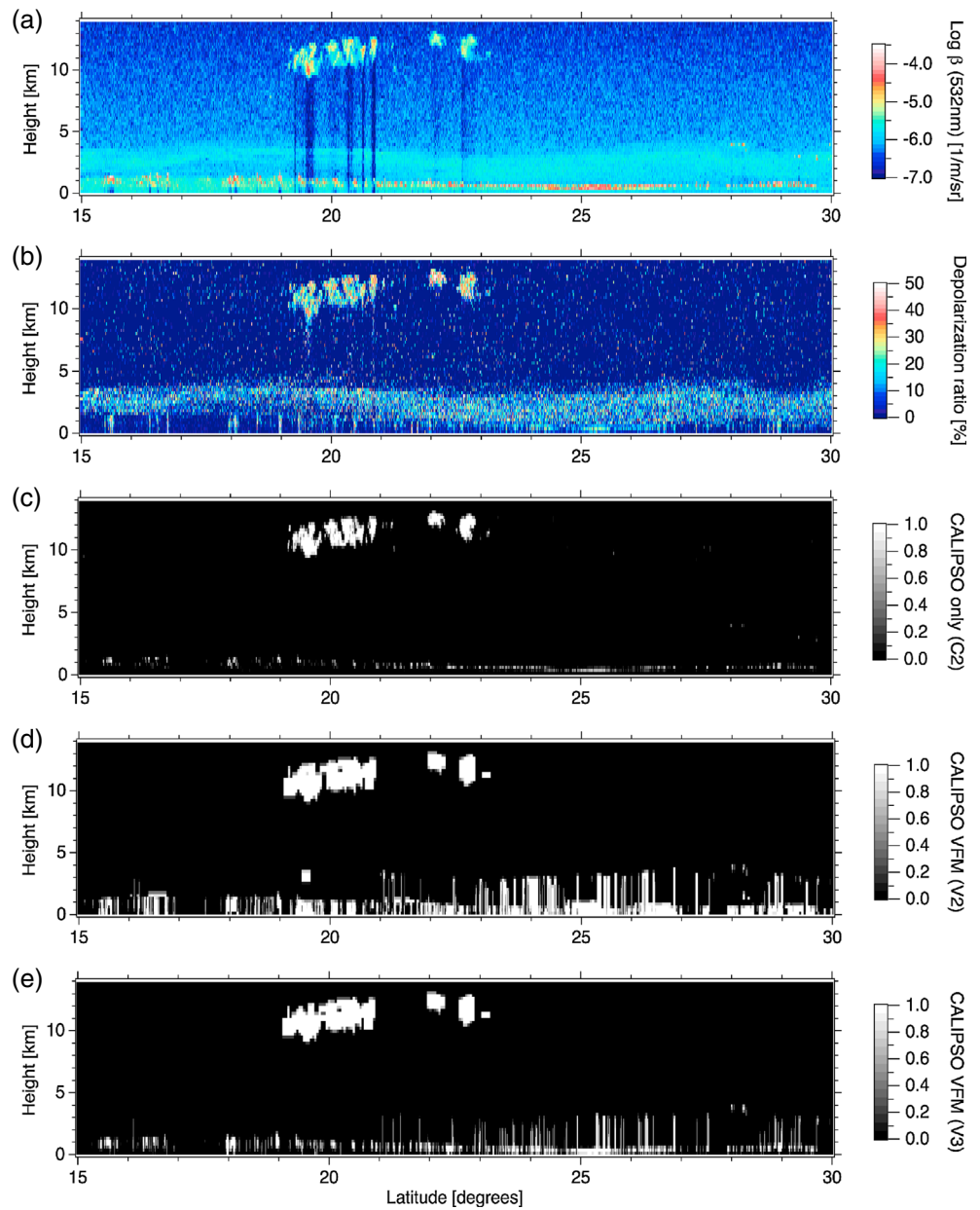


Figure 1. Latitude-height plot of (a) CALIPSO logarithm of 532 nm total backscatter (version 3, V3) over the North Atlantic Ocean on 8 October 2006; (b) depolarization ratio (V3); and cloud mask results from (c) CALIPSO only (C2, using V3), (d) the VFM (version 2, V2), and (e) the VFM (V3). The vertical resolution is 240 m, and the horizontal resolution is 1.1 km.

misclassification at low levels, the VFM showed the largest cloud coverage in the middle and low latitudes. *Rossow and Zhang [2010]* compared the combined CloudSat-CALIPSO VFM cloud data set (CloudSat 2B-GEOPROF-LIDAR product) with the collocated International Satellite Cloud Climatology Project (ISCCP) [*Rossow and Schiffer, 1999*] results. They found large differences in low-level cloudiness, which they attributed to the misclassification of cloud-free pixels by the VFM. They also found that the same analysis using our C2 scheme significantly reduced the disagreement.

V3 of the VFM, which reduces these problems, has been released. We compared our cloud mask results with both the previous (V2) and the current (V3) releases of the VFM. The CloudSat Z_e , the CALIPSO lidar β at 532 nm, and the ECMWF data were also averaged to make their vertical and horizontal resolutions match the cloud mask results. Figure 1 shows an example of latitude-height cross sections of CALIPSO (V3) β at 532 nm,

Table 1. Characteristic Cloud Features for Each Cloud Type

Cloud Type	Cloud Features
Type 1	
Type 1a	CALIPSO (C2) CTH \geq CloudSat (C1) CTH + 480 m
Type 1b	CALIPSO (C2) CTH determined only
Type 2	
Type 2a	CloudSat (C1) CTH \geq CALIPSO (C2) CTH + 480 m
Type 2b	CloudSat (C1) CTH determined only ^a
Type 3	CloudSat (C1) CTH - CALIPSO (C2) CTH < 480 m

^aType 2b is considered to be determined due to the false detection by CloudSat CPR cloud mask. Thus, it is removed from the analysis.

the depolarization ratio, and the cloud mask results for C2. From Figure 1, it can be seen that the CALIPSO signal clearly captured cirrus clouds along with Saharan dust aerosols that were characterized by a high depolarization ratio (~20%) with small attenuation (Figure 1b). To compare the C2 with VFM results, we first made a binary version of the VFM at the original CALIPSO resolution. All bins with a feature-type flag equal to 2 (cloud) were set to 1, and the other bins were set to 0. This binary VFM

(V2 in Figure 1d and V3 in Figure 1e) was then averaged to match the resolution of the observables and our mask results. Both C2 (Figure 1c) and the averaged VFM (Figures 1d and 1e) successfully detected cirrus and boundary layer clouds. However, the averaged VFM (Figures 1d and 1e) misclassified dust as cloud in the range from 21°N to 29°N below ~4 km. The cloud-edge detection was a little greater in the averaged VFM data (Figures 1d and 1e; e.g., ~20°N at ~11 km) because of its horizontal averaging procedure. Besides the example shown in Figure 1, the VFM appeared to misclassify the remaining noise signals located in the attenuated areas as cloud (not shown).

We also examined the zonal-mean cloud fractions obtained for September–November 2006. The cloud fraction at a given altitude was defined as the number of cloud bins (mask values >0.5) divided by the total number of observations at that level. Thus, it is a three-dimensional value. After CALIPSO was updated from V2 to V3, the cloud fractions derived by the VFM dramatically decreased below ~2.5 km. However, there was little change in those derived using the C2 scheme. The cloud fraction still differed by as much as 20% between the VFM V3 and C2 schemes. The analysis by *Rossow and Zhang [2010]* mentioned above used the CALIPSO V2. However, no significant difference was found between the zonal-mean cloud fraction derived with C2 scheme using either V2 or V3, so it is expected that the results of the comparison between C2 and ISCCP still hold. These results suggest that the VFM V2 issues discussed above still remained in the current release (VFM V3), although the degree of the misidentification in the VFM V3 was smaller than for VFM V2. This might affect the results of CTH differences between CloudSat and CALIPSO.

The CTHs are defined as the top height of the highest cloud in each profile in this study. The three major types of clouds and their subtypes were defined in terms of the CTH differences between CloudSat and CALIPSO (Table 1). We use the CALIPSO V3 data for the following analyses. If CALIPSO has higher sensitivities to cloud top regions than CloudSat, we categorize the clouds as type 1. Among them, when the CTH derived from CALIPSO with the C2 mask is 480 m higher than the CTH derived from CloudSat with the C1 mask, the cloud is categorized as type 1a. Type 1b clouds are defined as those that are only detected by the CALIPSO C2 mask and not by CloudSat at all. On the other hand, when CloudSat has higher sensitivity to cloud top regions than CALIPSO, we categorize the clouds as type 2. Similarly, when the CloudSat (C1 mask)-derived CTH is higher than the CALIPSO (C2 mask)-derived CTH by more than 480 m, the cloud is categorized as type 2a. Type 2b clouds are those that are detected by the CloudSat C1 mask but not by the CALIPSO C2 mask. However, as we explain later, type 2b is considered to occur due to false detection by CloudSat and is hence removed from our analysis. Finally, type 3 is the case where both CTHs detected by CloudSat and CALIPSO are within 480 m of each other. The CPR emits a pulse of 3.3 μ s duration, leading to an original vertical resolution of 480 m, and the backscattered signal is then oversampled to provide a data resolution of 240 m. To avoid false cloud detection by this oversampling, we imposed a minimum difference of 480 m. Additionally, we only looked at cases with CTH differences less than 3 km to avoid multilayer clouds such as subvisible cirrus overlying low-level clouds. Furthermore, to filter out surface clutter, bins with altitude < surface elevation + 1 km are also excluded. By definition, there is only one type of cloud for each profile. We also sorted clouds by CTH into three height categories bounded by cloud top pressure (CTP) of 440 hPa and 680 hPa following the ISCCP: low, CTP > 680 hPa; middle, CTP 440–680 hPa; and high, CTP < 440 hPa.

Although type 2b clouds are sometimes found in the data set, this is probably due to false detection by the official CloudSat CPR cloud mask (e.g., surface clutter and/or spurious echo estimation, correction, and mask not working effectively, as reported by the CloudSat team and also partly described in *Tanelli et al. [2008]*).

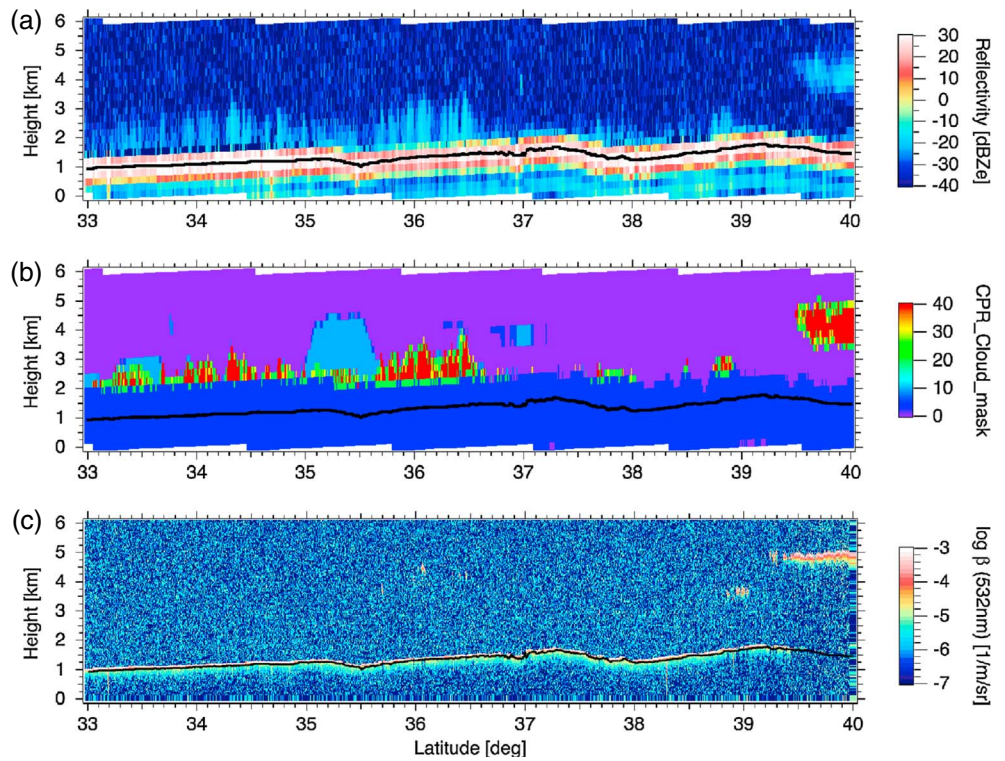


Figure 2. Latitude-height plot of (a) CloudSat reflectivity over the west coast of North America on 11 October 2006, (b) the CloudSat CPR cloud mask, and (c) the CALIPSO logarithm of 532 nm total backscatter. The resolution is the same as the original resolution of CloudSat and CALIPSO.

A latitude-height section of the CloudSat dBZ_e , CPR cloud mask, and CALIPSO β at 532 nm with original resolution is shown in Figure 2. We can see a weak echo (about -18 dBZ_e) over the strong surface clutter in the range from $33^\circ N$ to $39^\circ N$ below ~ 4 km (Figure 2a). The official CloudSat mask shows moderate or strong echoes (green or red regions in Figure 2b), i.e., regions where CloudSat detects clouds but CALIPSO does not (Figure 2c). This occurs over

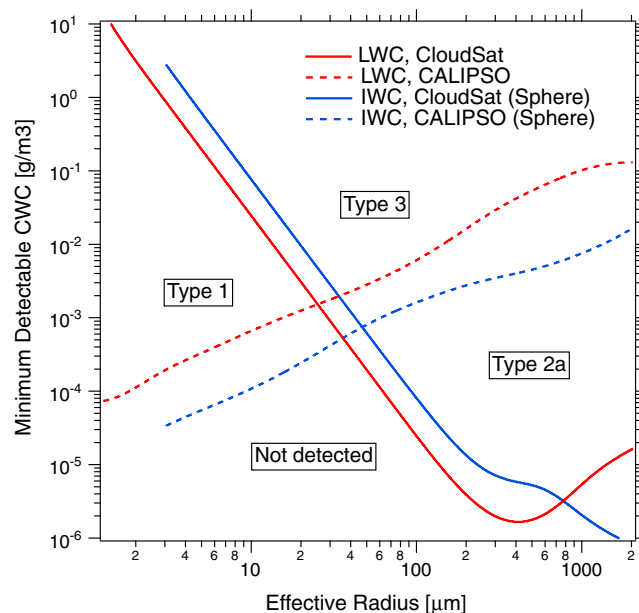


Figure 3. Minimum detectable cloud water content for CloudSat and CALIPSO.

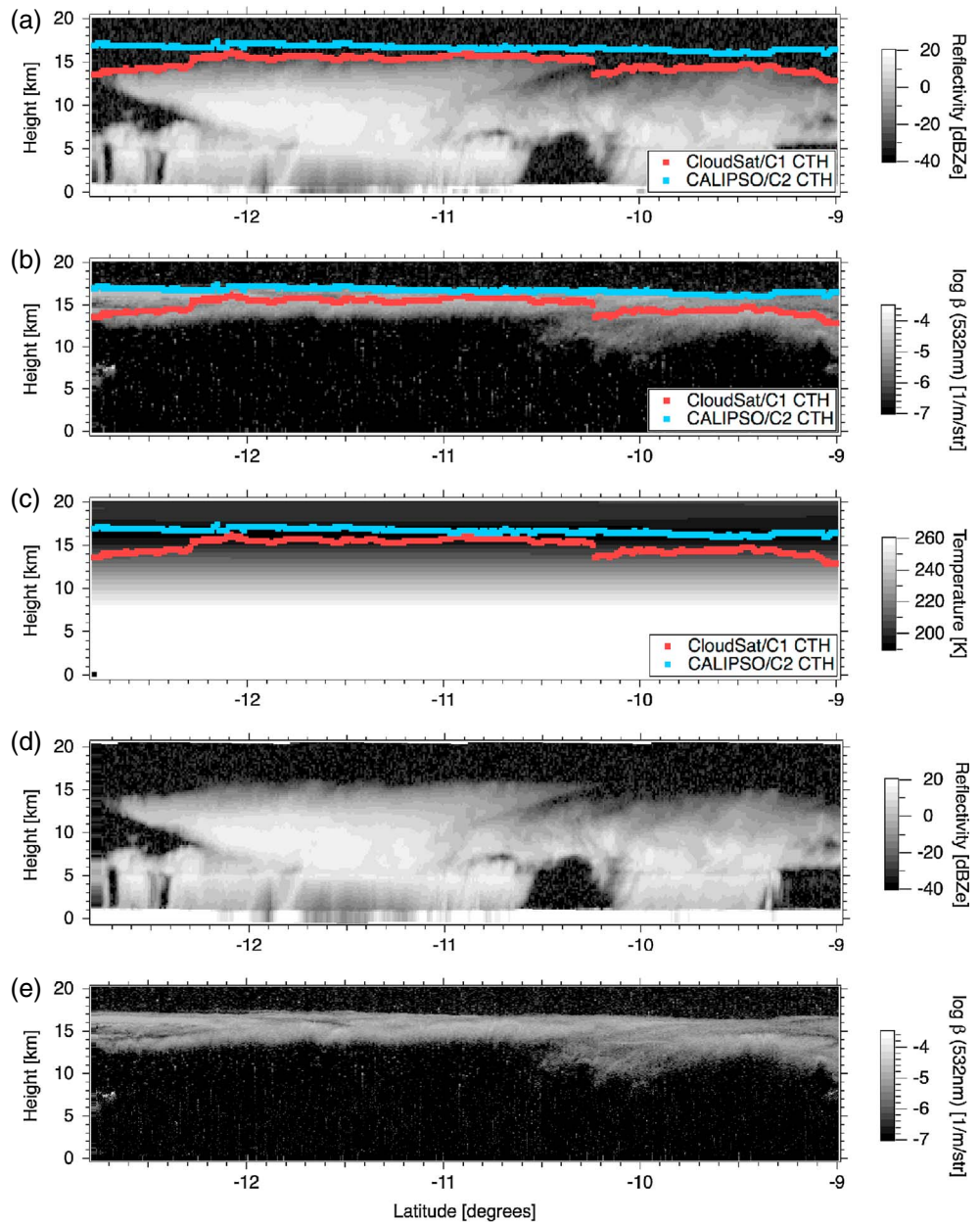


Figure 4. Latitude-height plot of (a) CloudSat reflectivity over Brazil on 30 October 2006, (b) CALIPSO logarithm of 532 nm total backscatter, and (c) ECMWF temperature. The resolution is 240 m in the vertical and 1.1 km in the horizontal. (d, e) Same as Figures 4a and 4b, but the resolution is the same as the original resolution of CloudSat and CALIPSO. The CTHs are determined by C1 (red) and C2 mask scheme (blue).

both land and ocean. It is difficult to physically justify the existence of such a scenario. Hence, type 2b clouds are omitted from the current analysis.

As mentioned in section 1, spaceborne cloud radar is more sensitive to large particles in the cloud tops than lidar, which is why CloudSat-derived CTH could be greater than that derived by CALIPSO. Here we theoretically estimate the minimum detectable liquid water content and ice water content as a function of the cloud effective radius r_e for CloudSat and CALIPSO (Figure 3). Look-up tables (LUTs) to retrieve ice cloud microphysics created by *Okamoto et al.* [2010] were used. The first one is for CloudSat Z_e and extinction coefficient for single randomly oriented crystal (3-D ice) particle category at 95 GHz. The second one is for CALIPSO and included β and extinction coefficient at 532 nm for 3-D ice category. Likewise, LUTs for water particle are made. These calculations are conducted by the Mie theory. The minimum sensitivity of CloudSat Z_{min} is about -30 dBZ_e

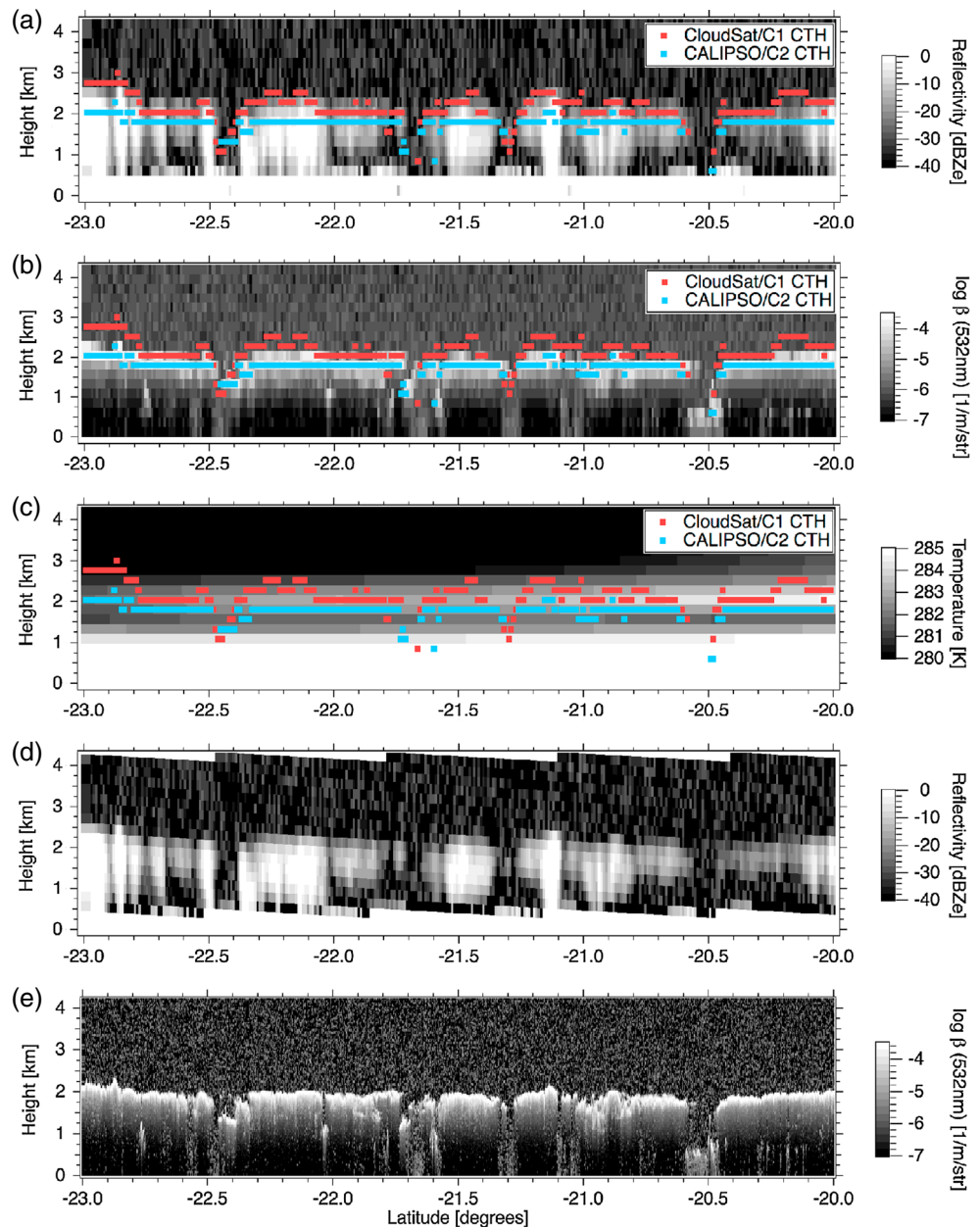


Figure 5. (a–e) As in Figure 4 but off Peru on 28 November 2006.

[Stephens *et al.*, 2008], and the minimum detectable β for CALIPSO is $10^{-5.25}$ (1/m/sr) for water clouds and is estimated to be about 10^{-6} (1/m/sr) for ice clouds by Hagihara *et al.* [2010]. Using these values, we estimated the minimum detectable cloud water content (CWC) through the LUTs. The results shown in Figure 3 indicate that CloudSat is more sensitive than CALIPSO to particles with r_e larger than about 25 μm for water and 50 μm for ice clouds, respectively. Therefore, if water particles with $r_e > 25 \mu\text{m}$ or ice particles with $r_e > 50 \mu\text{m}$ exist at the cloud tops, the clouds have a high probability of being classified as type 2a clouds. In contrast, when the particle size is smaller than this value, there is a high possibility of being classified as type 1 clouds. The areas below the lines are the undetected range.

3. Detection of Type 1 and Type 2 Clouds

Figures 4, 5, and 6 give examples of type 1a and type 2a clouds, showing (in Figures 4a–4c, 5a–5c, and 6a–6c) the latitude–height cross section of the CloudSat dBZ_e, the CALIPSO β at 532 nm, and the ECMWF temperature

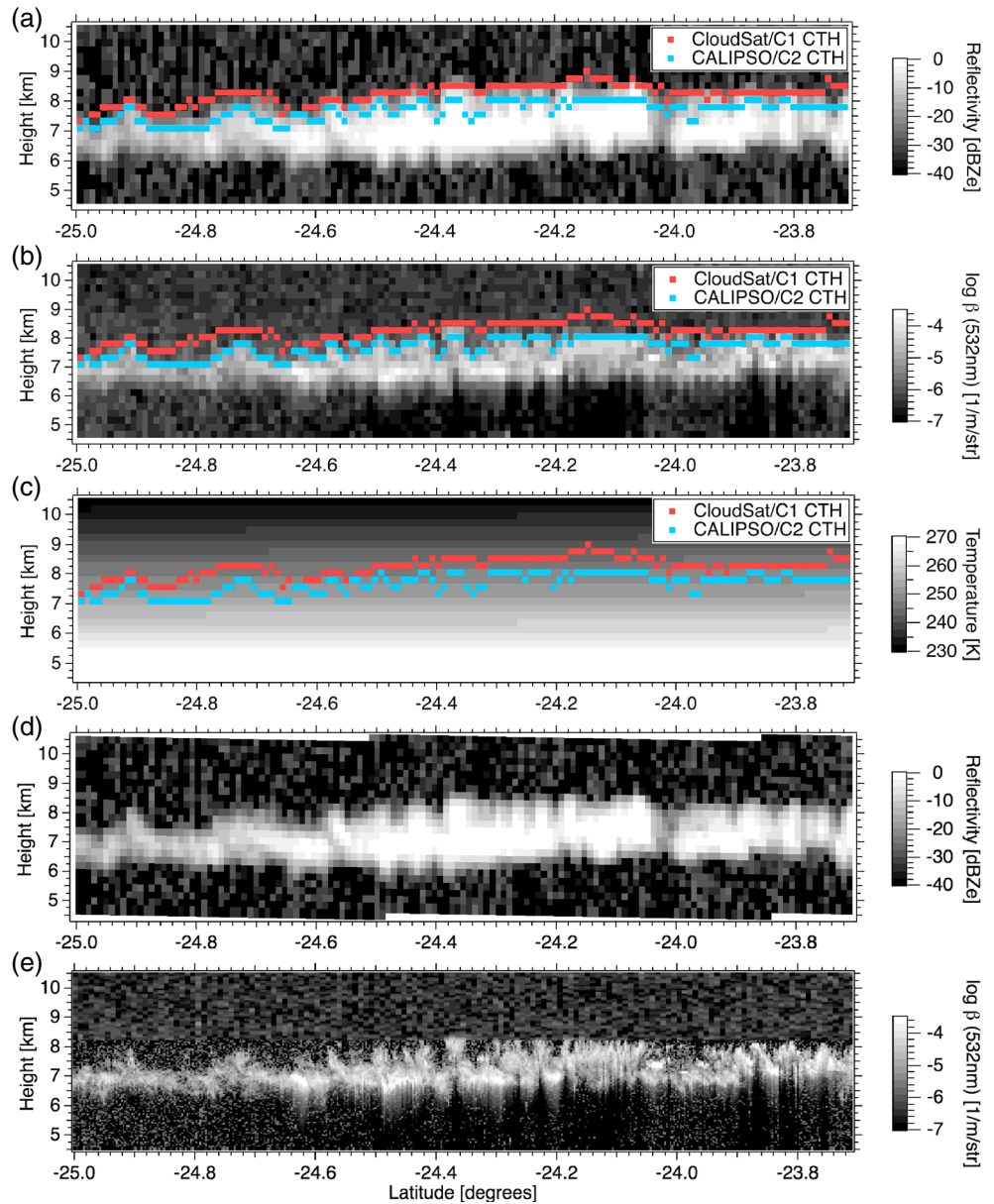


Figure 6. (a–e) As in Figure 4 but off the coast of Chile on 20 November 2006.

profile in gray. The CTHs determined by CloudSat (red dots) and CALIPSO (blue dots) are overlain in the panels. The dBZ_e and β in the original resolution are also shown in Figures 4d, 4e, 5d, 5e, 6d, and 6e.

The large high-level convective clouds located over Brazil on 30 October 2006 were categorized as type 1a, as shown in Figure 4. The observed dBZ_e and β values ranged from dark (no clouds) to white (strong backscatter from clouds). The clouds were categorized as 3-D ice according to a height-resolved cloud type classification method for CALIPSO (not shown) [Yoshida *et al.*, 2010]. In Figures 4a and 4b, the CALIPSO CTHs determined by our cloud masks are about 17 km, and the cloud top structure is flat, whereas the CloudSat CTHs are about 15 km. Overall, the CTHs derived by CALIPSO are about 1 ~ 3 km larger than those derived by CloudSat. This result is also confirmed in the original resolution (Figures 4d and 4e). At a latitude of around -10.0° , the CloudSat (CALIPSO) CTH is about 14.52 (16.44) km, the reflectivity at the CloudSat CTH is -25.52 dBZ_e , β at the CloudSat (CALIPSO) CTH is $10^{-5.27}$ ($10^{-5.65}$) (1/m/sr), and the CloudSat (CALIPSO) CTT is 201.45 (192.18) K. Although the environmental temperature at the CTH level determined by the ECMWF may not be exactly equal to the CTT [Luo *et al.*, 2009], we consider it the CTT because the difference should be small.

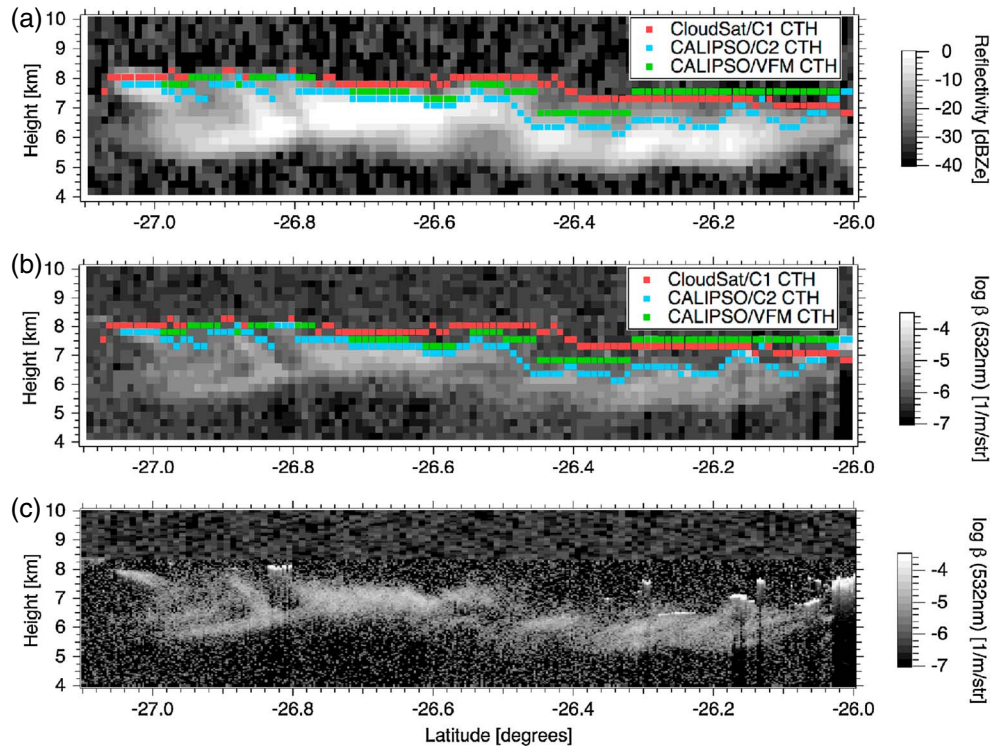


Figure 7. Latitude-height plot of (a) CloudSat reflectivity over the South Pacific Ocean and the northeast of New Zealand on 8 November 2006 and (b) CALIPSO logarithm of 532 nm total backscatter. The resolution is 240 m in the vertical and 1.1 km in the horizontal. (c) Same as Figure 7b, but the resolution is the same as the original resolution of CALIPSO. The CTHs are determined by C1 (red), C2 mask scheme (blue), and the VFM V3 (green).

An example of type 2a clouds is shown in Figure 5, where low-level clouds were located off the coast of Peru on 28 November 2006. Their particle type is warm water (not shown) [Yoshida *et al.*, 2010]. It is striking that the CTHs retrieved from CALIPSO are about 0.5 km lower than those retrieved by CloudSat on average (Figures 5a and 5b). We also confirm this behavior at the original resolution (Figures 5d and 5e). The CTHs determined using the C2 mask shown in Figure 5b seem to be somewhat lower than those at the original resolution illustrated in Figure 5e. The reason for this discrepancy lies in the criterion for cloud detection: Cloud fraction should exceed 0.5 on the averaged grids for CALIPSO and CloudSat. Near latitude -21° , the CTH determined by CloudSat (CALIPSO) is about 2.04 (1.56) km, the reflectivity at the C1 (C2) CTH is -22.25 (-11.26) dBZ_e , the β at the C2 CTH is $10^{-3.91}$ (1/m/sr), and the C1 (C2) CTT is 283.60 (281.91) K. Figure 5c shows that subsidence inversions occur. Interestingly, the upper part of the inversion layer is located near the CloudSat CTH level, while the lower part is at the CALIPSO CTH level.

Type 2a clouds were also found at higher level. Figure 6 shows high-level cirrus clouds on 20 November 2006, observed off the coast of Chile. The clouds mostly consist of 3-D ice, but supercooled water is also identified in the lower part (not shown) [Yoshida *et al.*, 2010]. The CloudSat CTHs are distinctively larger than the CALIPSO CTHs, as is clear from the averaged data set (Figures 6a and 6b). At a latitude of around -24.3° , the CTH determined by CloudSat (CALIPSO) is about 8.28 (7.56) km, the reflectivity at the C1 (C2) CTH is -16.71 (-6.37) dBZ_e , β at the C2 CTH is $10^{-4.39}$ (1/m/sr), and the C1 (C2) CTT is 246.17 (250.49) K. The CTHs differences are also confirmed at the original resolution, as demonstrated in Figures 6d and 6e.

The results derived from the VFM V3 instead of our C2 mask are interesting. Figure 7 shows a comparison of results with the VFM for type 2a clouds at high level on 8 November 2006 over the South Pacific Ocean and northeast of New Zealand. Figures 7a–7c show, respectively, the latitude-height cross section of the CloudSat dBZ_e and the CALIPSO β at 532 nm, along with β at 532 nm in the original resolution. In addition to the CTHs determined by CloudSat (red dots) and CALIPSO (blue dots), the CTHs determined by the averaged VFM (green dots) are also overlain on the panels. In the averaged data set (Figures 7a and 7b), the CTHs determined by the VFM are typically larger than those determined by our C2 mask. South of -26.3° latitude, the clouds are recognized as type 2a using the C1 and C2 CTHs, but not so using the C1 and VFM

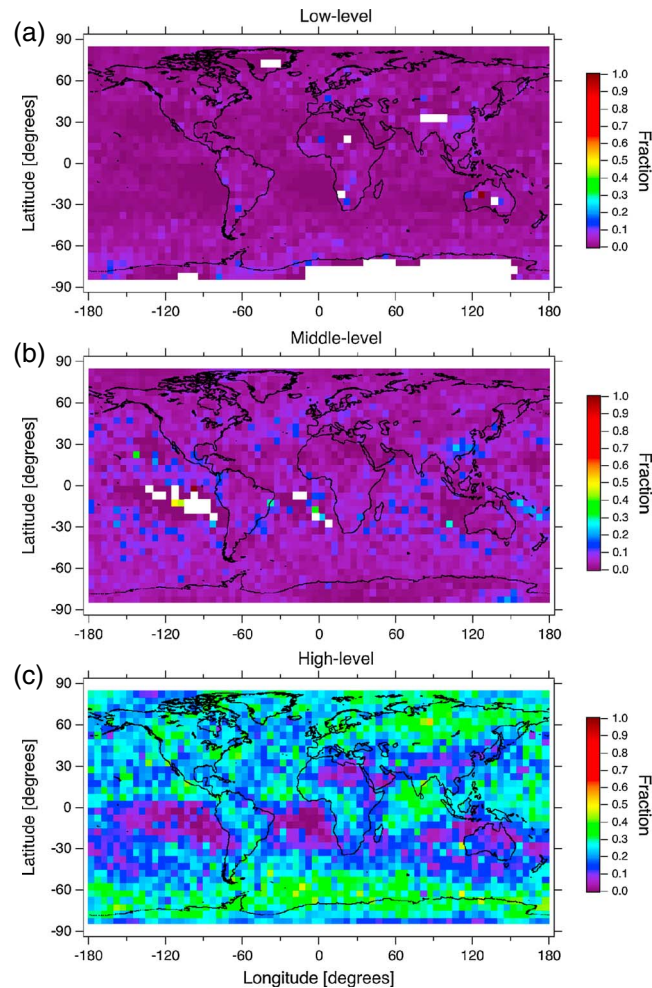


Figure 8. Fractional occurrence of type 1a clouds, for which the CALIPSO-determined cloud top heights (CTHs) were greater than those determined by CloudSat, categorized by the CTH during September–November 2006 at (a) low (surface to 680 hPa), (b) middle (680 hPa to 440 hPa), and (c) high (< 440 hPa) levels. The resolution is 5.0° latitude by 5.0° longitude.

CTHs, due to the overestimation of CTH in VFM results compared with the C2 mask, as confirmed at the original resolution (Figure 7c). As stated above, this overestimation is attributed to a misclassification as cloud by weak signals, which are often nearly indistinguishable from noise due to the horizontal averaging procedure of the VFM (~80 km). In both cases mentioned above (Figures 5 and 6), type 2a clouds are also observed using the VFM.

For the type 2a clouds, we believe that the top part of the clouds, which is detected by CloudSat but not by CALIPSO, consists of large particles with small number concentration (and small CWC) [Okamoto *et al.*, 2003] as discussed in section 2 through theoretical calculations. One possible explanation for the existence of large particles near the cloud top is as follows. An updraft first lifts both large particles and small particles aloft. Near the cloud top where cloud particles make contact with dry environment, evaporation starts to consume them. A larger fraction of the small particles gets entirely evaporated, while more of the large particles survive the evaporation process for a longer period of time. Subsequently, this selection procedure disproportionately preserves the large particles that are observed only by radar from space.

Marine cumulus and stratus clouds usually have in-cloud vertical air velocities V_{air} between $+0.1$ and $+0.6 \text{ m s}^{-1}$, where the positive sign indicates upward motion [e.g., Guibert *et al.*, 2003; Meskhidze *et al.*, 2005]. Peng *et al.* [2005] showed a cloud case that had $V_{air} \sim +0.7 \text{ m s}^{-1}$ with a temperature inversion using data from the Radiation, Aerosol and Cloud Experiment, whose resolution is 1 s in the temporal domain [Li *et al.*, 1998]. Because cloud particles have a terminal fall velocity V_t , one necessary condition for uplifting the particles

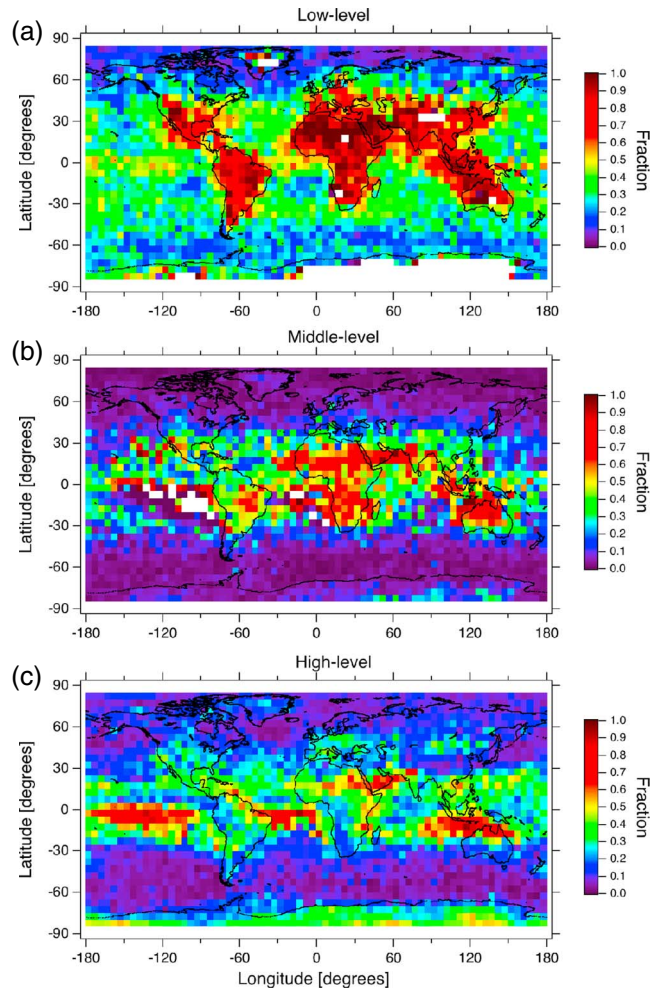


Figure 9. Fractional occurrence of type 1b clouds, for which the cloud top heights (CTHs) were only determined by CALIPSO, categorized by the CTH bounded by 440 and 680 hPa, during September–November 2006 at (a) low, (b) middle, and (c) high levels. The resolution is 5.0° latitude by 5.0° longitude.

discussed above is that the absolute value of V_{air} is larger than that of V_t . When the cloud is embedded in an environment with an upward V_{air} of $+0.7 \text{ m s}^{-1}$, the maximum size of r_e that results in $V_{air} + V_t = 0$ is estimated to be $\sim 55 \mu\text{m}$ following *Sato et al.* [2009] for an atmospheric temperature of 273 K and a pressure of 1000 hPa. Note that the V_t depends also on temperature and pressure so that the critical radius also varies for different environmental condition. This is consistent with the idea discussed above suggesting that CloudSat is more sensitive to water particles with $r_e > \sim 25 \mu\text{m}$ compared with CALIPSO. Up to this particle size and for the V_{air} value of $\sim +0.7 \text{ m s}^{-1}$, the water particles can therefore be lifted to near the cloud top and remain suspended in the air for some period of time, giving a greater chance for detection by CloudSat (but not by CALIPSO).

In the case of ground-based radar and lidar measurements, the radar echo top height is often higher than the lidar top height, but this is due to lidar attenuation. It is difficult to avoid the effect of attenuation for lidar in these cases, and hence it is difficult to see the real difference in CTH for radar and lidar. This study underscores the advantage of using spaceborne radar and lidar for studying cloud top microphysics and dynamics.

4. Global Distributions of Type 1 and Type 2 Clouds

4.1. Fractional Occurrence

We estimated the fractional occurrence of each cloud type (1a, 1b, and 2a), sorted by CTH, in three height categories during September–November 2006. The fraction in a grid box is defined as the number of each cloud

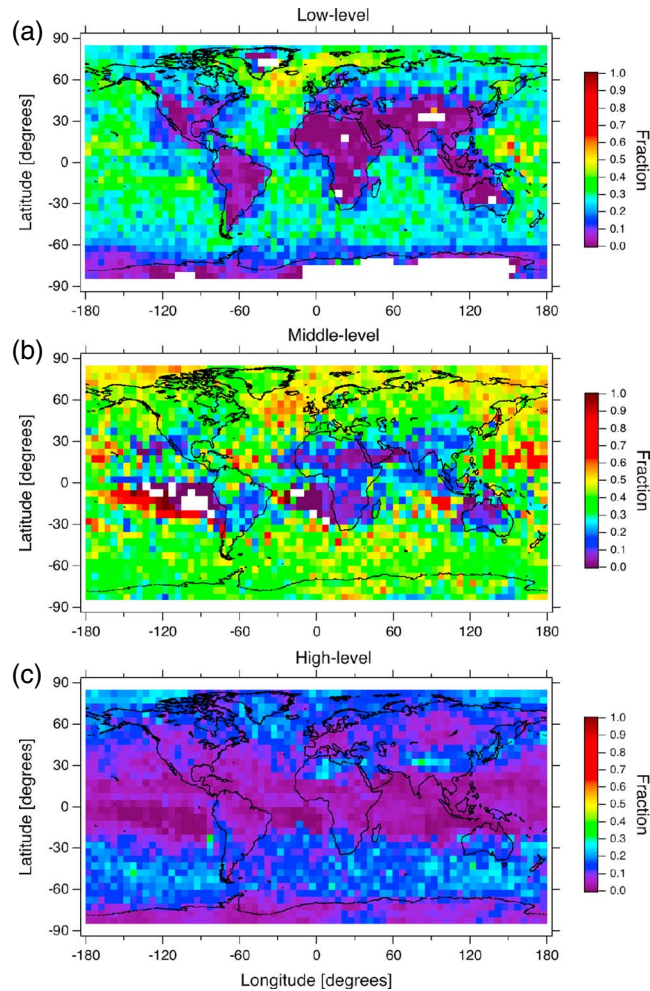


Figure 10. Fractional occurrence of type 2a clouds, for which CloudSat-determined cloud top heights (CTHs) are larger than those determined by CALIPSO, categorized by the CTH bounded by 440 and 680 hPa during September–November 2006 at (a) low, (b) middle, and (c) high levels. The resolution is 5.0° latitude by 5.0° longitude.

type profile (mask values >0.5) divided by the total number of profiles where CTHs could be determined by either C1 or C2 in a given grid box. The size of the grid box is set to be 5.0° latitude by 5.0° longitude to ensure that enough observations are collected for statistical analysis. The fraction of type 1 clouds is categorized into three height categories based on the C2 CTH, whereas the fraction of type 2a clouds is categorized based on the C1 CTH. If neither C1 nor C2 CTH is determined, the results are counted as missing values and are indicated in white.

Figure 8 shows the fraction of type 1a clouds for which the CALIPSO CTHs were greater than the CloudSat CTHs. There are almost no type 1a clouds at low level and midlevel because there are few clouds with small particles at the cloud tops, which could not be detected by radar (Figures 8a and 8b). Meanwhile, clouds consisting of small particles (e.g., cirrus clouds) that are detected by lidar but not radar are frequently present at high level [e.g., Heymsfield, 1986]. As expected, the type 1a clouds mostly occur at high level in all regions except for the subtropical high (~35%; Figure 8c).

Figure 9 shows the fraction of type 1b clouds for which only CALIPSO detects cloud. At low level and midlevel, larger fractions of type 1b than of type 1a clouds are found, especially over land at low latitudes and midlatitudes (Figures 9a and 9b). These clouds are composed of small particles that can be only detected by lidar, such as shallow cumulus that do not contain drizzle droplets. Such clouds seem to be more prevalent over land than over ocean. We also see from Figure 9c that type 1b clouds are present at high level in the tropics and over Antarctica. This may be caused by the presence of thin cirrus and polar stratospheric clouds (PSCs) in which small particles are dominant [e.g., Adhikari et al., 2010].

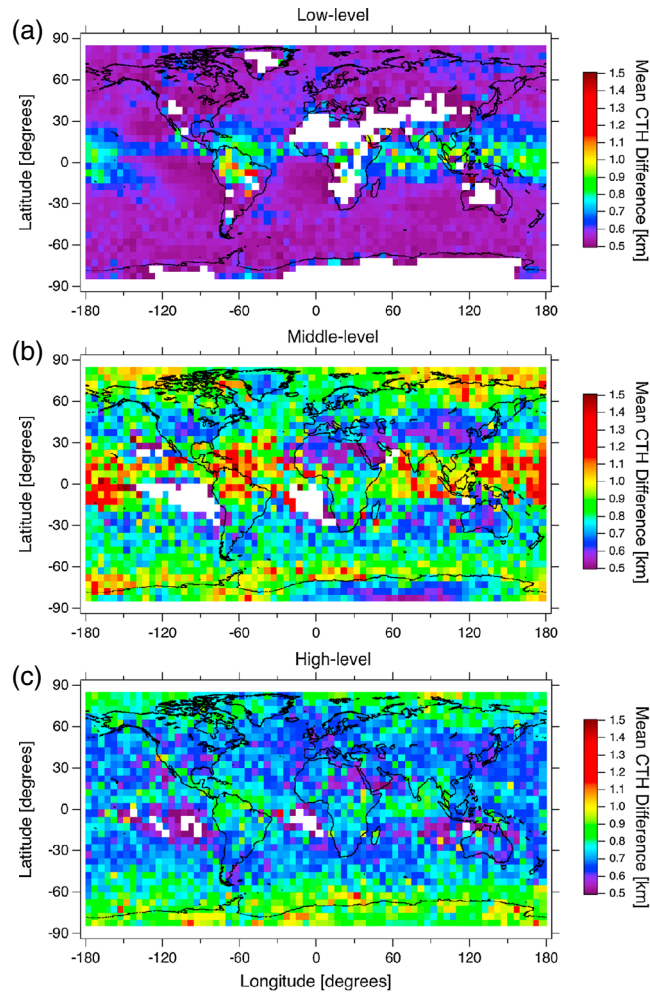


Figure 11. Type 2a mean cloud top height (CTH) differences (CTH by C1 – CTH by C2), categorized by the CTH bounded by 440 and 680 hPa during September–November 2006 at (a) low, (b) middle, and (c) high levels. The resolution is 5.0° latitude by 5.0° longitude.

The global distribution of the fraction of type 2a clouds for which CloudSat CTHs are greater than CALIPSO CTHs is examined (Figure 10). In Figure 10a, a large fraction is present at low level, particularly over the ocean on the western coasts of the continents, in the midlatitude storm track regions, and over the North Atlantic Ocean (~40%). Type 2a clouds also appear at midlevel over the whole area and are especially prominent over ocean, except for part of the subtropical high region (Figure 10b). It should be emphasized that this is the first time that type 2a clouds are revealed from space by joint analysis of CloudSat and CALIPSO lidar observations. Traditional wisdom (i.e., lidar is more sensitive to clouds than radar is) will only lead to the type 1 clouds. At low level, significant differences are revealed between land and ocean: The type 2a fraction (Figure 10a) was larger (smaller) over ocean (land), whereas a countertendency was found in the type 1 (=1a + 1b) fraction (Figures 8a and 9a). This suggests that the low-level clouds have relatively large (small) particles in the cloud top region over ocean (land). This might have been caused by the differences in cloud formation and/or the abundance of aerosols serving as cloud condensation nuclei between land and ocean due to the aerosol indirect effects, as proposed by Twomey [1977] and Albrecht [1989]. These phenomena were confirmed on a global scale by several previous studies [e.g., Nakajima *et al.*, 2001; Bréon *et al.*, 2002].

4.2. CTH Differences

The CTH differences (CTH by C1 – CTH by C2) for type 2a sorted by the C1 CTHs are shown in Figure 11. By definition, only positive values appear. Interestingly, at low level, small values (roughly 0.55 km) are found over the whole area (except the Intertropical Convergence Zone (ITCZ), central South America, the tropical Indian Ocean, and tropical west Pacific). We can also see somewhat larger differences around the ITCZ

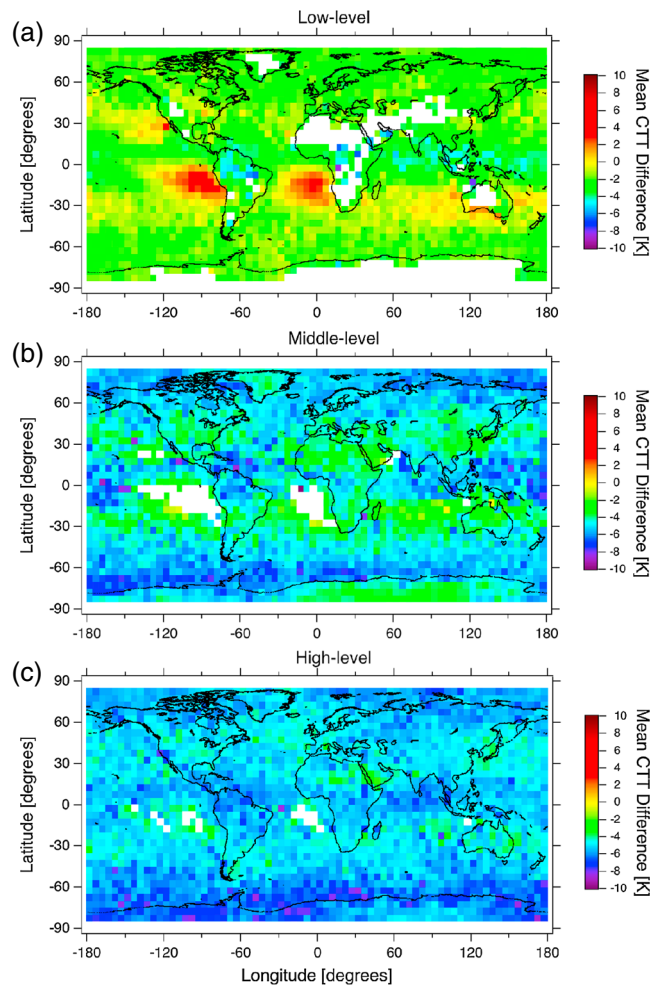


Figure 12. Type 2a mean cloud top temperature (CTT) differences (CTT by C1 – CTT by C2), categorized by the CTH bounded by 440 and 680 hPa during September–November 2006 at (a) low, (b) middle, and (c) high levels. The resolution is 5.0° latitude by 5.0° longitude.

probably caused by a strong updraft within convection. At midlevel, up to 1.65 km differences are found over the whole area, except for part of the subtropical high region, especially in the region of the ITCZ and poles. For high-level clouds, the CTH differences are similar in magnitude to those of the low-level clouds and are smaller than those of the midlevel clouds. There seems to be little regional differences, except the relatively large values in the polar region. The reasons for these polar features are not immediately clear to us.

4.3. CTT Differences

Similar analyses are conducted for CTT associated with type 2a clouds, as shown in Figure 12. The CTT differences (CTT by C1 – CTT by C2) are calculated for three height categories in terms of the C1 top heights. In the case study for low-level clouds as shown in Figure 5, the type 2a clouds existed within the inversions. Interestingly, we can also see from Figure 12a that the differences are actually positive (about 6 K) for low-level clouds over some regions, mostly near the western coasts of continents (California, Peru, and Guinea). It is well known that temperature inversions occur over these regions [e.g., Klein and Hartmann, 1993]. At midlevel, the CTT difference is about –3 K in most regions. These negative differences are also found at high level in regions similar to the midlevel but with smaller values.

4.4. Global Statistics

The global statistics are summarized in Table 2. The definition of the fraction of each type was the number of each cloud type profile (mask values >0.5) divided by the total number of profiles, where the CTHs were determined by either C1 or C2 in each height category. The cloud coverage was defined as the number of

Table 2. Global Statistics for Fractional Cloud Occurrence, the Mean Cloud Top Height Difference, and the Mean Cloud Top Temperature Difference for Each Cloud Type^a

Total (Land/Ocean)	Type 1 (=1a + 1b)	Type 1a (C2 CTH > C1)	Type 1b (C2 CTH only)	Type 2a (C1 CTH > C2)	Type 3 (C1 CTH = C2)	Cloud Coverage
<i>Fraction</i>						
Low (>680 hPa)	0.31 (0.41/0.29)	0.02 (0.03/0.02)	0.29 (0.38/0.27)	0.26 (0.19/0.27)	0.43 (0.40/0.43)	0.14 (0.05/0.18)
Mid (440–680 hPa)	0.15 (0.19/0.12)	0.04 (0.04/0.04)	0.11 (0.15/0.08)	0.39 (0.36/0.41)	0.43 (0.43/0.43)	0.09 (0.10/0.08)
High (0–440 hPa)	0.45 (0.49/0.43)	0.24 (0.25/0.24)	0.21 (0.24/0.19)	0.10 (0.09/0.11)	0.30 (0.26/0.32)	0.37 (0.38/0.37)
<i>Mean CTH difference [km]</i>						
Low (>680 hPa)		0.79 (0.79/0.78)		0.56 (0.57/0.56)		
Mid (440–680 hPa)		1.29 (1.20/1.34)		0.86 (0.82/0.88)		
High (0–440 hPa)		1.33 (1.40/1.30)		0.76 (0.76/0.76)		
<i>Mean CTT difference [K]</i>						
Low (>680 hPa)		−3.53 (−3.78/−3.48)		−1.33 (−2.21/−1.23)		
Mid (440–680 hPa)		−7.29 (−6.95/−7.48)		−5.19 (−4.85/−5.36)		
High (0–440 hPa)		−9.29 (−9.63/−9.10)		−5.49 (−5.45/−5.51)		

^aThe cloud coverage for which either CloudSat or CALIPSO can detect cloud top heights, except for the clouds only detected by CloudSat, is also shown. The results of comparisons over land and ocean are shown in parentheses. CTH, cloud top height; CTT, cloud top temperature.

profiles whose CTHs were determined by either C1 or C2 divided by the total number of profiles in each height category. Thus, it is a two-dimensional value.

In Table 2, the fractions of types 1a, 1b, 2a, and 3 clouds at low level are 2, 29, 26, and 43%, respectively. Surprisingly, the type 2a clouds account for 26% of the total globally, making them the third largest type. The type 1b fraction is 29% in this height category, which indicates the percentage of clouds that CloudSat misses completely. Because water clouds usually consist of small particles, type 1b clouds that only CALIPSO can detect are a large fraction of the total. The fractions of types 1b and 2a show large differences over land and over ocean probably due to the aerosol indirect effect, as noted earlier. At midlevel, types 1a, 1b, 2a, and 3 clouds show fractions of 4, 11, 39, and 43%, respectively. Type 2a is the second largest type. Type 1a is the smallest fraction (only 4% among these types in the height category). Type 1b is relatively minor at midlevel. At high level, types 1a, 1b, 2a, and 3 clouds have fractions of 24, 21, 10, and 30%, respectively. The fraction of type 1a is large (24%) at high level, as was type 3. Meanwhile, type 2a represents a relatively small fraction (10%). These results reflect the fact that the cloud top part of the high clouds mostly consists of small particles.

The product of the fraction times the cloud cover in a height category gives the absolute value of the frequency of occurrence for a type. The absolute values of the frequency of occurrence of type 1 (=1a + 1b) and type 2a clouds are 4% and 4% at low level, 1% and 4% at midlevel, and 17% and 4% at high level, respectively. Because the type 2a clouds are not always accompanied by inversions, as seen in Figure 12a, the mean CTT differences in type 2a at low level are negative (~ -1.33 K).

4.5. Inhomogeneity Effects

As described above, we used the C2 mask results (0–1) to determine C2 CTHs. Our C2 mask scheme is first applied to CALIPSO data in original resolution. Then the results are averaged so that the resolutions match those of the (ideal) CloudSat grid. In each profile, the highest bin that had the C2 averaged mask values exceeding the threshold value of 0.5 was considered C2 cloud top. If cloud top is very fuzzy and inhomogeneous within the CloudSat grid scale (240 m in vertical and 1.1 km horizontal), CALIPSO may give some different readings on CTH. Thus, the overestimation of type 2 cloud fraction might occur owing to inhomogeneous C2 cloud tops within the corresponding CloudSat grid. We conducted the sensitivity analysis by considering the C2 threshold value as a proxy for assessing how inhomogeneous the CALIPSO cloud tops in the original resolution across the corresponding CloudSat grid are. For example, the C2 CTHs determined by the C2 threshold value >0.8 are almost unaffected by the inhomogeneity. On the other hand, the CTHs by the threshold value >0.0 and <0.2 were significantly affected by the inhomogeneity. We investigated the number of profiles by changing the C2 threshold in three cases (>0.5 :current, >0.8 :small inhomogeneity, and <0.2 :large inhomogeneity) categorized by CTH and surface type. The results show that the number of profiles of current cases is comparable to the number of small inhomogeneity cases and they are much larger than the number of

Table 3. Radar/Lidar Signals and Microphysics

	β (a) > β (b)	β (a) < β (b)
dBZ _e (a) > dBZ _e (b)	CWC (a) > CWC (b)	r_e (a) > r_e (b)
dBZ _e (a) < dBZ _e (b)	r_e (a) < r_e (b)	CWC (a) < CWC (b)

inhomogeneity cases. Therefore, we concluded that the inhomogeneity of cloud structure does not play a significant role in the statistics.

4.6. Using VFM V3 Instead of C2

We also examined the global statistics when we used the VFM V3 instead of our C2 mask. At low level, the fraction of type 2a clouds becomes 17%, which is smaller than our results by 9%. In contrast, the fraction of type 1b clouds that is only detected by CALIPSO at low level becomes larger than our results. These differences can be explained as follows. As noted previously, the VFM misclassifies the remaining noise and aerosols as clouds and has horizontal averaging up to 80 km. This might have led to overestimation of the cloud fraction compared with our scheme. As a result, the type 2a clouds are less pronounced when the VFM is used. Our C2 scheme avoids these issues and better captures the existence of the type 2a clouds, because the root reason for type 2a cloud, namely, patches of large cloud particles occurring near cloud top, is probably a small-scale phenomenon (smaller than 80 km) that is associated with updraft as large as 0.7 m s^{-1} (see section 3).

4.7. Impact of Keeping Type 2b Clouds

We also investigated the fraction of type 2b clouds that were omitted from the analysis described above. The frequency of occurrence of type 2b clouds is 18% at low level, 10% at midlevel, and 1% at high level. The fraction of type 2a clouds when type 2b is considered becomes 22% at low level, 35% at midlevel, and 10% at high level. This suggests that removal of spurious clouds detected by CloudSat CPR cloud mask is important, especially for low-lying clouds.

5. Analyses of Z_e and β in Relation to Cloud Types

The differences in CTHs between CloudSat and CALIPSO, i.e., the sensitivities to cloud top regions, reflects cloud microphysics in the cloud top regions. The different types bear information on different cloud microphysical properties, such as r_e and CWC. To infer the differences in cloud microphysics, we compare Z_e and β in cloud top regions between the CTHs detected by radar and lidar for each type. For constant CWC, Z_e and β are approximately proportional to r_e^3 and r_e^{-1} , respectively. Z_e and β are proportional to CWC when r_e is constant [Okamoto *et al.*, 2003]. Then, the cloud microphysics can be inferred from comparisons between the two signals. We first discuss four scenarios where both Z_e and β signals exist in cloud regions between the two CTHs. The relationships between two ideal kinds of signals, as represented by (a) and (b), and the corresponding microphysics are summarized in Table 3. There, (a) and (b) denote two arbitrarily chosen cloud regions just for the sake of comparison. Four scenarios with different combinations of dBZ_e and β are as follows.

1. When both the dBZ_e and β values for cloud region (a) are larger than those for cloud region (b), the following can be inferred: Larger dBZ_e signals imply that the r_e values of (a) are larger and/or that the CWC of (a) is larger than that of CWC (b), whereas larger β values in (a) imply that the r_e values in (a) are smaller and/or that the CWC in (a) is larger than the CWC in (b). Therefore, we concluded that the CWC in (a) is larger than the CWC in (b) in this scenario.
2. Following a similar argument, when the value of dBZ_e is larger in (a) but β is smaller in (a), the r_e values in (a) are larger than those in (b), but we cannot infer CWC.
3. When the dBZ_e is smaller in (a) and β is larger in (a), it can be inferred that the value of r_e in (a) is smaller than that in (b).
4. Finally, when both the dBZ_e and β values are smaller in (a), the CWC in (a) is smaller than that in (b), following the same reasoning as in scenario (1).

We also consider the observables from CloudSat and CALIPSO when there is only one signal, i.e., type 1 or 2a. For type 1 clouds, β is observed but Z_e for the cloud region is below the Z_{min} . In such cases, Z_{min} can be used as an upper limit for the cloud region. Similarly, for type 2a clouds, Z_e is observed but β is below the detectable

Table 4. Cloud Types and Microphysics

	$dBZ_e > dBZ_e$ (Type 3)	$dBZ_e < dBZ_e$ (Type 3)	$\beta > \beta$ (Type 3)	$\beta < \beta$ (Type 3)
Type 1 ($dBZ_e < dBZ_{e, min} < dBZ_e$ (type 3))	-	-	$r_e < r_e$ (type 3)	$CWC < CWC$ (type 3)
Type 2a ($\beta < \beta_{th} < \beta$ (type 3))	$r_e > r_e$ (type 3)	$CWC < CWC$ (type 3)	-	-

threshold, so the threshold value of β can be used as upper limits for type 2a clouds. For the type 3 clouds, both Z_e and β are obtained for the same cloud regions. It might then be possible to compare the cloud microphysics of each type, as summarized in Table 4.

Comparisons of the frequency distributions of Z_e categorized by the CTHs are shown in Figure 13. We can only compare types 2a and 3 because type 1 does not have detectable Z_e (see second row in Table 4). Type 2a clouds are dominant at low level and midlevel (26 and 39%, respectively) compared with high level (10%), as shown in section 4 (Table 2). Figure 13 shows that the type 2a clouds have a somewhat wider distribution than the type 3 clouds, with slightly larger frequency at larger dBZ_e , i.e., > -12 dBZ_e for low level and midlevel and > -19 dBZ_e for the high level. This suggests that the cloud top of type 2a consists of relatively larger

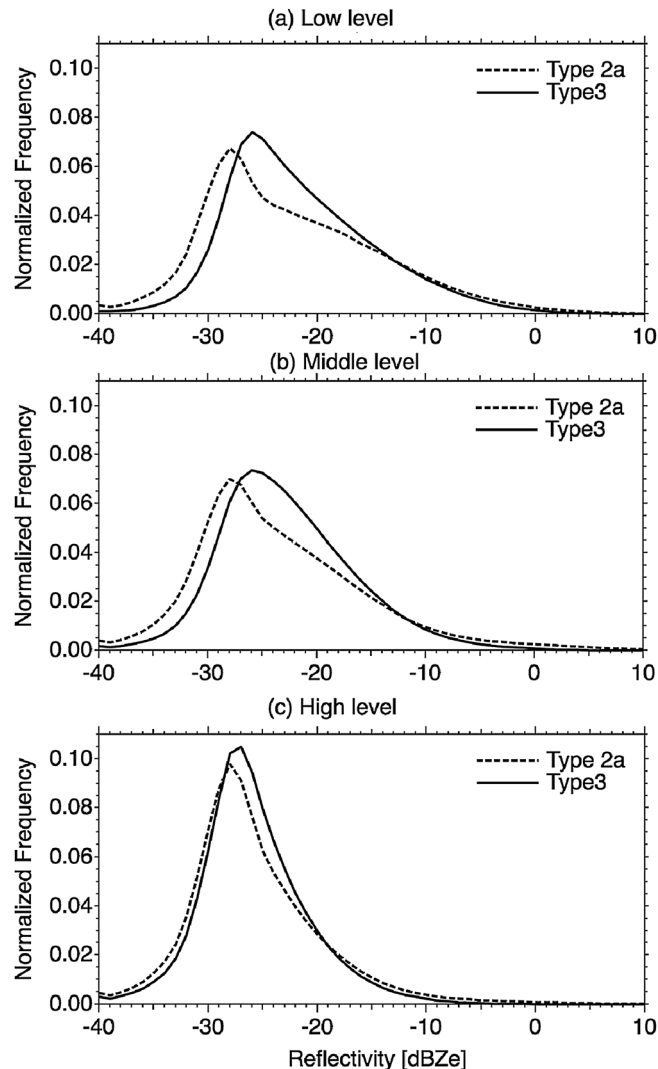


Figure 13. Frequency distribution comparison for CloudSat reflectivity for types 2a and 3, categorized by CTH bounded by 440 and 680 hPa during September–November 2006 at (a) low, (b) middle, and (c) high levels.

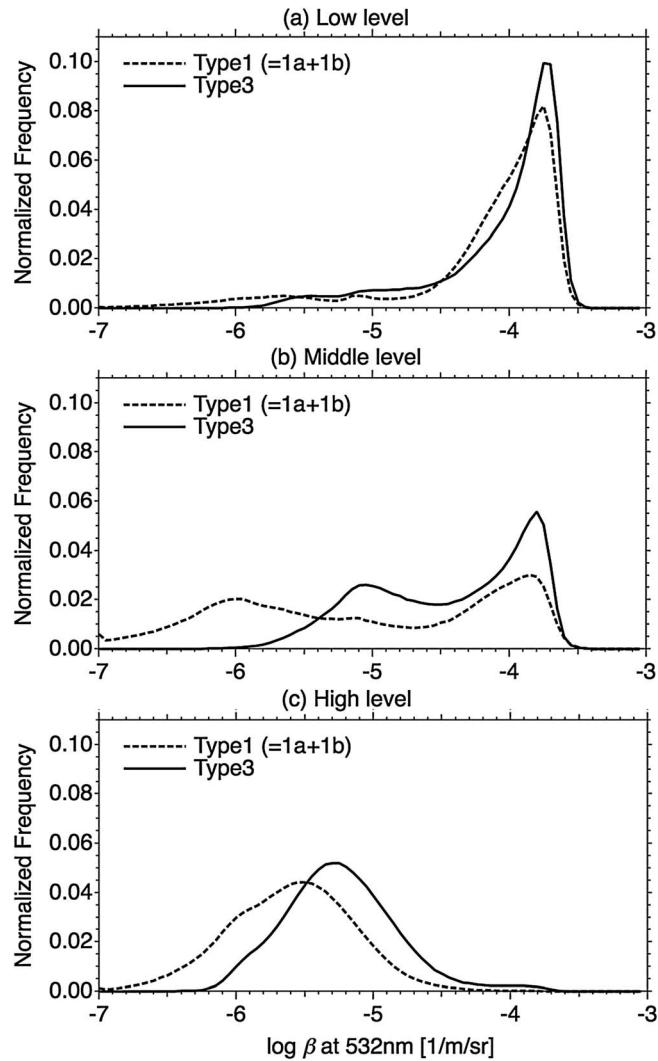


Figure 14. Frequency distribution comparison of the CALIPSO logarithm of 532 nm total backscatter for types 1 (=1a + 1b) and 3, categorized by CTHs bounded by 440 and 680 hPa during September–November 2006 at (a) low, (b) middle, and (c) high levels.

particles than that of type 3 because Z_e depends on particle size at the first order, which supports our hypothesis as discussed in section 3. Meanwhile, the locations of maximum dBZ_e occurrence for type 2a ($\sim -28 \text{ dBZ}_e$) are smaller than those for type 3, i.e., $\sim -25 \text{ dBZ}_e$ for low level and midlevel, whereas they show little difference at high level. The mode value of β in type 2a is below the threshold value of β (β_{th}), and that of type 3 is larger ($\sim 10^{-3.8} \text{ (1/m/sr)}$; Figures 14a and 14b) than β_{th} , i.e., β of type 2a is smaller than that of type 3. When both observables (dBZ_e and β) are smaller, this means that CWC of type 2a is smaller than that of type 3 for low level and midlevel, as mentioned earlier.

Similar comparisons are made for β at 532 nm (Figure 14). This was possible only for types 1 (1a + 1b) and 3 because type 2a does not have detectable β (see first row in Table 4). The type 1 clouds are relatively abundant at high level (45%; see Table 2). Figure 14 shows that at low level, the peak value of the frequency distributions for types 1 and 3 are located at $\beta = 10^{-3.8} \text{ (1/m/sr)}$. This large peak is also found at midlevel (Figure 14b) but not at high level (Figure 14c). We therefore conclude that this value corresponds to water clouds. Besides, both types 1 and 3 had a high frequency around $\beta = 10^{-5.2}$ and 10^{-6} (1/m/sr) at midlevel, respectively, and type 3 also had a former peak at high level, which we attribute to ice clouds and the PSCs. Figure 14c shows that type 1 had a mode $\beta = 10^{-5.5} \text{ (1/m/sr)}$, which was smaller than that of type 3 in the high-level clouds. Additionally, the mode value of Z_e for type 1 was below Z_{min} , but that of type 3 was larger

(-27 dBZ_e; Figure 13c) than Z_{\min} . When both observables (dBZ_e and β) are smaller, this indicates that the CWC of type 1 is smaller than that of type 3.

6. Summary

A joint analysis of CloudSat and CALIPSO lidar was conducted to study cloud top heights and microphysics. The CTHs were determined by a cloud mask scheme for CloudSat (C1) and CALIPSO (C2) [Hagihara *et al.*, 2010]. We introduced three cloud types and their subtypes. The type 1 clouds are those for which C2 CTHs are greater than C1 CTHs (type 1a), or CTHs are only detected by C2 (type 1b). The type 2 clouds are those for which C1 CTHs are greater than C2 CTHs (type 2a). Because the clouds only detected by C1 (type 2b) are likely spurious due to false detection by the CloudSat CPR cloud mask, we excluded these clouds from our analysis. Type 3 is the case where both C1 and C2 detect the CTHs. The global statistics were analyzed using the C2 and also the VFM. We also compared the frequency distribution of observables (i.e., dBZ_e and β) to infer the characteristic of microphysics in cloud top regions. The main findings of this paper are the following:

1. The fraction of type 1a clouds is relatively large (~35%) at high level in all regions as expected. A major "surprise" of the study is the finding that type 2a clouds are unexpectedly common. These cases frequently occurred at low level and midlevel over the ocean along the western coasts of continents, mid-latitude storm tracks, and the North Atlantic Ocean. These results seem to suggest that the cloud top part of the low-level and midlevel clouds in these regions often consists of large particles. The global mean fractions of type 2a clouds are 26% and 39% at low level and midlevel, respectively, and the corresponding CTH differences were 0.56 and 0.86 km, respectively. This is considered a new discovery that was first revealed by our joint analysis of CloudSat and CALIPSO. It underscores the fact that the CTHs cannot be determined by satellite-borne lidar only; better results come from the combined use of radar and lidar. Temperature inversions occurred over the western coasts of continents (California, Peru, and Guinea), and the CTT differences are about 6 K in those regions.
2. The problems in the previous release (version 2, V2) of the CALIPSO VFM are still found in the current release (version 3, V3), although the degree of misidentification in V3 is smaller than in VFM V2. In the VFM results, the fraction of type 2a clouds is 17% at low level, which is smaller than in our results by 9%. In contrast, the fraction of clouds that are only detected by CALIPSO at low level is larger than in our results. The VFM misclassifies the remaining noise and aerosols as clouds. High horizontal averaging (up to 80 km) might have led to the overestimation of cloud fraction compared with our scheme. Consequently, type 2a clouds are less pronounced in the VFM. In this study, our C2 scheme, which avoids these issues, better captures and characterizes the type 2a clouds.
3. Type 2a clouds show a wider Z_e frequency distribution than the type 3 clouds. Larger occurrence frequencies are found for type 2a at larger dBZ_e, i.e., > -12 dBZ_e at low level and midlevel and > -19 dBZ_e at high level. This implies that the cloud top region of type 2a clouds consists of relatively larger particles than that of type 3. The CWC is found to be smaller for type 1 ($=1a + 1b$) and 2a clouds compared with type 3 clouds. These findings support our hypothesis about type 2a clouds, namely, such cloud top regions consist of large particles with small number concentration. The simultaneous measurement from space, especially a Doppler cloud radar and a high-spectral resolution lidar onboard the Earth Cloud, Aerosol and Radiation Explorer, will help us further explore detailed cloud formation mechanisms along with the effect on the Earth radiation budget of these cloud top conditions.

Acknowledgments

We thank W. B. Rossow of City College of New York and K. Sato of Kyushu University for their helpful advice. We are grateful to the CloudSat and CALIPSO science teams and engineers whose efforts and commitment made this study possible. This work was partly supported by the Ministry of Education, Culture, Sports, Science and Technology of Japan through Grant-in-Aid for Scientific Research B (22340133) and A (25247083); by the Special Coordination Fund for Promoting Science and Technology of the Japanese Cloud Seeding Experiments for Precipitation Augmentation (JCSEPA); by the Collaborative Research Program of Research Institute for Applied Mechanics, Kyushu University, through the Study on influences of the global warming and rapid economic growth on the marine and atmospheric environment in the East Asia; and by the GRENE Arctic Climate Change Research Project. Z.L. acknowledges support from NASA under grants NNX10AM31G and NNX12AC13G.

References

- Ackerman, S. A., R. E. Holz, R. Frey, E. W. Eloranta, B. C. Maddux, and M. McGill (2008), Cloud detection with MODIS. Part II: Validation, *J. Atmos. Oceanic Technol.*, *25*, 1073–1086, doi:10.1175/2007JTECHA1053.1.
- Adhikari, L., Z. Wang, and D. Liu (2010), Microphysical properties of Antarctic polar stratospheric clouds and their dependence on tropospheric cloud systems, *J. Geophys. Res.*, *115*, D00H18, doi:10.1029/2009JD012125.
- Albrecht, B. A. (1989), Aerosols, cloud microphysics, and fractional cloudiness, *Science*, *245*, 1227–1230, doi:10.1126/SCIENCE.245.4923.1227.
- Bréon, F.-M., D. Tanré, and S. Generoso (2002), Aerosol effect on cloud droplet size monitored from satellite, *Science*, *295*, 834–838.
- Guibert, S., J. R. Snider, and J.-L. Brenguier (2003), Aerosol activation in marine stratocumulus clouds: 1. Measurement validation for a closure study, *J. Geophys. Res.*, *108*(D15), 8628, doi:10.1029/2002JD002678.
- Hagihara, Y., H. Okamoto, and R. Yoshida (2010), Development of a combined CloudSat–CALIPSO cloud mask to show global cloud distribution, *J. Geophys. Res.*, *115*, D00H33, doi:10.1029/2009JD012344.
- Haynes, J. M., T. S. L'Ecuyer, G. L. Stephens, S. D. Miller, C. Mitrescu, N. B. Wood, and S. Tanelli (2009), Rainfall retrieval over the ocean with spaceborne W-band radar, *J. Geophys. Res.*, *114*, D00A22, doi:10.1029/2008JD009973.

- Heymsfield, A. (1986), Notes and correspondence: Ice particles observed in a cirriform cloud at -83°C and implications for polar stratospheric clouds, *J. Atmos. Sci.*, *43*, 851–855.
- Holz, R. E., S. A. Ackerman, F. W. Nagle, R. Frey, S. Dutcher, R. E. Kuehn, M. A. Vaughan, and B. Baum (2008), Global Moderate Resolution Imaging Spectroradiometer (MODIS) cloud detection and height evaluation using CALIOP, *J. Geophys. Res.*, *113*, D00A19, doi:10.1029/2008JD009837.
- Klein, S. A., and D. L. Hartmann (1993), The seasonal cycle of low stratiform clouds, *J. Clim.*, *6*(8), 1587–1606.
- Li, S., K. B. Strawbridge, W. R. Leitch, and A. M. Macdonald (1998), Aerosol backscattering determined from chemical and physical properties and lidar observations over the east coast of Canada, *Geophys. Res. Lett.*, *25*, 1653–1656, doi:10.1029/98GL00910.
- Liu, Z., M. Vaughan, D. Winker, C. Kittaka, B. Getzewich, R. Kuehn, A. Omar, K. Powell, C. Trepte, and C. Hostetler (2009), The CALIPSO lidar cloud and aerosol discrimination: Version 2 algorithm and initial assessment of performance, *J. Atmos. Oceanic Technol.*, *26*, 1198–1213, doi:10.1175/2009JTECHA1229.1.
- Luo, Z., G. Y. Liu, G. L. Stephens, and R. H. Johnson (2009), Terminal versus transient cumulus congestus: A CloudSat perspective, *Geophys. Res. Lett.*, *36*, L05808, doi:10.1029/2008GL036927.
- Mace, G. G., Q. Q. Zhang, M. Vaughan, R. Marchand, G. Stephens, C. Trepte, and D. Winker (2009), A description of hydrometeor layer occurrence statistics derived from the first year of merged Cloudsat and CALIPSO data, *J. Geophys. Res.*, *114*, D00A26, doi:10.1029/2007JD009755.
- Mahesh, A., M. A. Gray, S. P. Palm, W. D. Hart, and J. D. Spinhirne (2004), Passive and active detection of clouds: Comparisons between MODIS and GLAS observations, *Geophys. Res. Lett.*, *31*, L04108, doi:10.1029/2003GL018859.
- Marchand, R., G. G. Mace, T. Ackerman, and G. Stephens (2008), Hydrometeor detection using Cloudsat—An Earth-orbiting 94-GHz cloud radar, *J. Atmos. Oceanic Technol.*, *25*, 519–533, doi:10.1175/2007JTECHA1006.1.
- Menzel, W. P., R. A. Frey, H. Zhang, D. P. Wylie, C. C. Moeller, R. E. Holz, B. Maddux, B. A. Baum, K. I. Strabala, and L. E. Gumley (2008), MODIS global cloud-top pressure and amount estimation: Algorithm description and results, *J. Appl. Meteorol. Climatol.*, *47*, 1175–1198, doi:10.1175/2F2007JAMC170z5.1.
- Meskhidze, N., A. Nenes, W. C. Conant, and J. H. Seinfeld (2005), Evaluation of a new cloud droplet activation parameterization with in situ data from CRYSTAL-FACE and CSTRIFE, *J. Geophys. Res.*, *110*, D16202, doi:10.1029/2004JD005703.
- Nakajima, T., A. Higurashi, K. Kawamoto, and J. E. Penner (2001), A possible correlation between satellite-derived cloud and aerosol microphysical parameters, *Geophys. Res. Lett.*, *28*, 111–1174.
- Okamoto, H., S. Iwasaki, M. Yasui, H. Horie, H. Kuroiwa, and H. Kumagai (2003), An algorithm for retrieval of cloud microphysics using 95-GHz cloud radar and lidar, *J. Geophys. Res.*, *108*(D7), 4226, doi:10.1029/2001JD001225.
- Okamoto, H., et al. (2007), Vertical cloud structure observed from shipborne radar and lidar: Midlatitude case study during the MR01/K02 cruise of the research vessel Mirai, *J. Geophys. Res.*, *112*, D08216, doi:10.1029/2006JD007628.
- Okamoto, H., T. Nishizawa, T. Takemura, K. Sato, H. Kumagai, Y. Ohno, N. Sugimoto, A. Shimizu, I. Matsui, and T. Nakajima (2008), Vertical cloud properties in the tropical western Pacific Ocean: Validation of the CCSR/NIES/FRCGC GCM by shipborne radar and lidar, *J. Geophys. Res.*, *113*, D24213, doi:10.1029/2008JD009812.
- Okamoto, H., K. Sato, and Y. Hagihara (2010), Global analysis of ice microphysics from CloudSat and CALIPSO: Incorporation of specular reflection in lidar signals, *J. Geophys. Res.*, *115*, D22209, doi:10.1029/2009JD013383.
- Peng, Y., U. Lohmann, and R. Leitch (2005), Importance of vertical velocity variations in the cloud droplet nucleation process of marine stratus clouds, *J. Geophys. Res.*, *110*, D21213, doi:10.1029/2004JD004922.
- Rossow, W. B., and R. A. Schiffer (1999), Advances in understanding clouds from ISCCP, *Bull. Am. Meteorol. Soc.*, *80*, 2261–2287, doi:10.1175/1520-0477(1999)080<2261:AIUCFI>2.0.CO;2.
- Rossow, W. B., and Y. Zhang (2010), Evaluation of a statistical model of cloud vertical structure using combined CloudSat and CALIPSO cloud layer profiles, *J. Clim.*, *23*, 6641–6653, doi:10.1175/2010JCLI3734.1.
- Sassen, K., and Z. Wang (2008), Classifying clouds around the globe with the CloudSat radar: 1-year of results, *Geophys. Res. Lett.*, *35*, L04805, doi:10.1029/2007GL032591.
- Sato, K., H. Okamoto, M. K. Yamamoto, S. Fukao, H. Kumagai, Y. Ohno, H. Horie, and M. Abo (2009), 95-GHz Doppler radar and lidar synergy for simultaneous ice microphysics and in-cloud vertical air motion retrieval, *J. Geophys. Res.*, *114*, D03203, doi:10.1029/2008JD010222.
- Stephens, G. L. (1999), Radiative effects of clouds and water vapor, in *Global Energy and Water Cycle*, edited by K. A. Browning and R. J. Gurney, pp. 71–90, Cambridge Univ. Press, New York.
- Stephens, G. L., et al. (2002), The CloudSat mission and A-train, *Bull. Am. Meteorol. Soc.*, *83*, 1771–1790, doi:10.1175/BAMS-83-12-1771.
- Stephens, G. L., et al. (2008), CloudSat mission: Performance and early science after the first year of operation, *J. Geophys. Res.*, *113*, D00A18, doi:10.1029/2008JD009982.
- Tanelli, S., L. Durden, E. Im, K. S. Pak, D. G. Reinke, P. Partain, J. M. Haynes, and R. T. Marchand (2008), CloudSat's cloud profiling radar after two years in orbit: Performance, calibration, and processing, *IEEE Trans. Geosci. Remote Sens.*, *46*, 3560–3573.
- Twomey, S. (1977), Influence of pollution on shortwave albedo of clouds, *J. Atmos. Sci.*, *34*, 1149–1152, doi:10.1175/1520-0469(1977)034<1149:TIOPTO>2.0.CO;2.
- Vaughan, M. A., K. A. Powell, R. E. Kuehn, S. A. Young, D. M. Winker, C. A. Hostetler, W. H. Hunt, Z. Liu, M. J. McGill, and B. J. Getzewich (2009), Fully automated detection of cloud and aerosol layers in the CALIPSO lidar measurements, *J. Atmos. Oceanic Technol.*, *26*, 2034–2050, doi:10.1175/2009JTECHA1228.1.
- Weisz, E., J. Li, W. P. Menzel, A. K. Heidinger, B. H. Kahn, and C. Y. Liu (2007), Comparison of AIRS, MODIS, CloudSat and CALIPSO cloud top height retrievals, *Geophys. Res. Lett.*, *34*, L17811, doi:10.1029/2007GL030676.
- Winker, D. M., M. A. Vaughan, A. H. Omar, Y. Hu, K. A. Powell, Z. Liu, W. H. Hunt, and S. A. Young (2009), Overview of the CALIPSO mission and CALIOP data processing algorithms, *J. Atmos. Oceanic Technol.*, *26*, 2310–2323, doi:10.1175/2009JTECHA1281.1.
- Wu, D. L., et al. (2009), Vertical distributions and relationships of cloud occurrence frequency as observed by MISR, AIRS, MODIS, OMI, CALIPSO, and CloudSat, *Geophys. Res. Lett.*, *36*, L09821, doi:10.1029/2009GL037464.
- Wylie, D., E. Eloranta, J. D. Spinhirne, and S. P. Palm (2007), Comparison of cloud cover statistics from the GLAS lidar with HIRS, *J. Clim.*, *20*, 4968–4981, doi:10.1175/JCLI4269.1.
- Yoshida, R., H. Okamoto, Y. Hagihara, and H. Ishimoto (2010), Global analysis of cloud phase and ice crystal orientation from Cloud–Aerosol Lidar and Infrared Pathfinder Satellite Observation (CALIPSO) data using attenuated backscattering and depolarization ratio, *J. Geophys. Res.*, *115*, D00H32, doi:10.1029/2009JD012334.